Analytica Chimica Acta 1135 (2020) 64–72

Contents lists available at ScienceDirect

Analytica Chimica Acta

journal homepage: www.elsevier.com/locate/aca

A path-choice-based biosensor to detect the activity of the alkaline phosphatase as the switch

Jiarui Zhang [a, 1], Wenbo Zhao [b, 1], Wei Zhang [c, d], Yizhou Liu [c], Yang Qin [c], Wenkai Zhang [c], Zhiyuan Zhou [a], Yujie Zhou [a], Hongbo Wang [d], Xianjin Xiao [a, c, d, **], Tongbo Wu [a, c, *]

[a] School of Pharmacy, Tongji Medical College, Huazhong University of Science and Technology, Wuhan, 430030, China
[b] State Key Laboratory of NBC Protection for Civilian, Beijing, 102205, China
[c] Institute of Reproductive Health/Center of Reproductive Medicine, Tongji Medical College, Huazhong University of Science and Technology, Wuhan, 430030, China
[d] Department of Obstetrics and Gynaecology, Union Hospital, Tongji Medical College, Huazhong University of Science and Technology, Wuhan, 430022, China

HIGHLIGHTS

- A path-choice-based biosensor (PCB) is designed with DNA tracks and λ exonuclease.
- Alkaline phosphatase (ALP) as the switch controls the path-choice behaviour of PCB.
- Substrate preference of ALP and λ exonuclease is studied to optimize DNA tracks.
- Simple, fast, sensitive and selective detection of ALP is achieved with PCB.

GRAPHICAL ABSTRACT

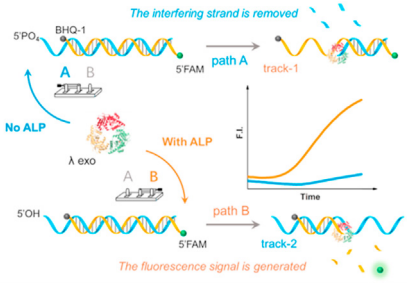

ARTICLE INFO

Article history:
Received 14 June 2020
Received in revised form
19 August 2020
Accepted 23 August 2020
Available online 27 August 2020

Keywords:
Alkaline phosphatase
Lambda exonuclease
Path-choice
Fluorescent detection
Biosensor

ABSTRACT

Alkaline phosphatase (ALP), which converts the phosphate group (-PO_4) in the substrate to the hydroxyl group (-OH), is a useful tool in the biological analysis, a good indicator of dissolved inorganic phosphorus levels and an important biomarker for several diseases. In conventional designs for ALP detection, both the interferent with a -PO_4 and the target with a −OH will go into the sensing path and give out the undesired background and the desired signal respectively. This limited the sensitivity of the method and required the complicated design to achieve a satisfying limit of detection (LOD) of ALP. Here, we provided a new sensing strategy for ALP detection design. We designed a path-choice-based biosensor with two DNA tracks in which ALP works as the switch to guide the reaction path of lambda exonuclease (λ exo). The path-choice character enlarged the difference between signal and background by separating the interferent removing path and the target sensing path. The substrate preference of ALP and λ exo was studied to optimize the structure of DNA tracks. The path-choice-based biosensor achieved simple, fast (30 min), sensitive (LOD 0.014 U L^{-1}) and selective detection of the activity of ALP. The method has been

* Corresponding author. School of Pharmacy, Tongji Medical College, Huazhong University of Science and Technology, Wuhan, 430030, China.
** Corresponding author. Institute of Reproductive Health/Center of Reproductive Medicine, Tongji Medical College, Huazhong University of Science and Technology, Wuhan, 430030, China.
E-mail addresses: xiaoxianjin@hust.edu.cn (X. Xiao), wutongbo@hust.edu.cn (T. Wu).
[1] These authors contributed equally to this work.

https://doi.org/10.1016/j.aca.2020.08.040
0003-2670/© 2020 Elsevier B.V. All rights reserved.

applied to detect the activity of ALP in cell lysates, which shows the potential application in ALP-related biological research.

© 2020 Elsevier B.V. All rights reserved.

1. Introduction

Alkaline phosphatase (ALP), an essential enzyme to catalyze the dephosphorylation reaction [1], is extensively used to provide the signal for the analytes in the biological analysis such as immunoassays [2,3], histochemical staining [4] and aptamer-based assay [5]. In these biological analysis methods, ALP could be labelled on the secondary antibody or streptavidin. When the analyte presents, ALP will be remained or released to participate in the subsequent reaction and generate the signal. Thus, the detection of the analyte could be converted to the detection of ALP. Potentially all the proteins and enzymes that have the corresponding antibody or aptamer could be detectable using ALP labelling. Multiple proteins, enzymes, and even small molecules [6–11] have been detected using ALP to generate the signal. In these biological analyses, the detection limit of the analyte is highly related to the detection limit of ALP, and sensitive detection of ALP could improve the detection sensitivity of these assays. Moreover, ALP is a good indicator of dissolved inorganic phosphorus (DIP) levels. The detection of ALP could serve as a warning sign of algal bloom in eutrophic water bodies [12–14]. Also, ALP could be used as a crucial biomarker of disease diagnosis. The abnormally high level of ALP in serum is proven to be highly related to several diseases, including bone diseases, liver dysfunction, prostate cancer, breast cancer, and diabetes [15]. Also, hypophosphatasia, hypothyroidism, anemia and other conditions or diseases may lead to reduced levels of ALP [16]. Therefore, it's necessary and significant to develop reliable and sensitive methods to detect ALP for related biological researches.

Until now, many methods have been developed to quantify ALP activity, such as colorimetric method [17], surface enhancement Raman scattering [18], chromatography [19] and electrochemistry [20]. However, these methods inevitably suffer from one or more limitations, such as poor sensitivity, complicated design, expensive materials, and time-consuming procedures. Recently, more and more efforts have been put into fluorescent analysis to overcome these disadvantages because of its high sensitivity, convenience and accessible instruments. One strategy is using organic or inorganic probes (such as carbon dots and quantum dots) which could give out signal directly in response of ALP. However, these methods still have drawbacks. For example, the organic molecular probes suffer from poor sensitivity (LOD: 0.15–60 U L^{-1}) [12,21–23]. Carbon dots are limited by the complicated preparation process [24]. Quantum dots made by metal are usually biologically toxic [25–27]. Another promising strategy is using phosphate labelled DNA to build fluorescent sensors. After ALP digestion, the phosphate is converted to the hydroxyl. The hydroxyl will trigger downstream reactions and generate fluorescent signals [28–38]. However, the existing methods with high sensitivity for ALP detection need relatively long detection time or special components (materials or enzymes) that would impede their applications in biological researches. Also, most of the existing methods for ALP detection ignored to discuss their selectivity to nucleases that always appear in the biological matrixes such as serum and cell lysate.

In conventional designs for ALP detection (Scheme 1), there is only one path to generate the signal. The interferent strand with a phosphate group (-PO_4) and the target strand with a hydroxyl group (-OH) will both go into the sensing path and give out the undesired background and the desired signal respectively. Thus, the difference between the background and signal is only related to the selectivity of -PO_4 over −OH. For example, Lambda exonuclease (λ exo) is an exonuclease with 5'→3′ cleavage activity [39]. It prefers the double-stranded DNA (dsDNA) substrate with 5′-PO_4 over that without 5′-PO_4 (5′-OH). Thus, λ exo is used for ALP detection in several works. However, the selectivity of λ exo to 5′-PO_4 and 5′-OH is limited. The LOD of these methods ranges from 0.01 U L^{-1} to 40 U L^{-1} [40–44] even with complicated signal amplification designs.

In this work, we designed a novel path-choice-based biosensor (PCB) to detect the activity of ALP, which will act as the switch in the system. Unlike conventional designs, in the PCB, there are two paths for λ exo to choose (Fig. 1). Without ALP, λ exo chooses Path A and removes the interfering strand, which produces the background in conventional designs. With ALP, λ exo chooses the sensing path (Path B) and generate a strong fluorescent signal. Thus, the difference between signal and background could be enlarged, and the activity of ALP could be sensitively detected without complicated designs. Also, the method shows good selectivity and could be applied in biological samples.

2. Material and methods

2.1. Materials

The DNA oligonucleotides (oligos) used in this work were synthesized and purified by Sangon Biotech Co. (Shanghai, China). The sequences of all the oligos were listed in Table 1. Calf intestinal alkaline phosphatase (ALP), bovine serum albumin (BSA), DNase I, T7 exonuclease (T7 exo), Exonuclease III (Exo III), Uracil glycosylase (UDG), and CutSmart reaction buffer (50 mM KAc, 20 mM Tris-Ac, 10 mM $Mg(Ac)_2$, 100 μg/ml BSA, pH 7.9 @ 25 °C) were purchased from New England Biolabs (MA, USA). Lambda exonuclease (λ exo) and λ exo buffer (67 mM Glycine-KOH, 2.5 mM $MgCl_2$, 50 μg/ml BSA, pH 9.4 @ 25 °C) were purchased from ThermoFisher Scientific (MA, USA). All the DNA oligos were synthesized and purified by Sangon Biotech Co. (Shanghai, China). The concentration of DNA oligonucleotides was measured by NanoDrop 2000 UV–vis Spectrophotometer (ThermoFisher Scientific).

2.2. Selection of reaction buffer (Fig. S2)

5 μL of the probe (2.5 pmol), 5 μL of the C-strand-7nt (2.5 pmol), 35 μL of water and buffer (5 μL of 10 × CutSmart buffer, 5 μL of 10 × CutSmart buffer and mixture of 2.5 μL of 10 × CutSmart buffer and 2.5 μL of 10 × λ exo buffer) after heating and annealing were added to 400 μL ELISA plate, respectively. 1 μL of ALP (7.5×10^{-5} U) and 2 μL of λ exo (1 U) were added at the same time. Then put the plate into Synergy HTX instrument (BioTek, American) for fluorescence measurement. The fluorescence intensity was recorded at 37 °C in the period of 30 s for 20 min, and the gain level was 60. The excitation and absorption wavelengths were set to 485 nm and 582 nm, respectively.

2.3. Optimization of the reaction of time (Fig. S3)

5 μL of the probe (2.5 pmol), 5 μL of the C-strand-7nt (2.5 pmol), 2.5 μL of 10 × CutSmart buffer and 2.5 μL of 10 × λ exo buffer and

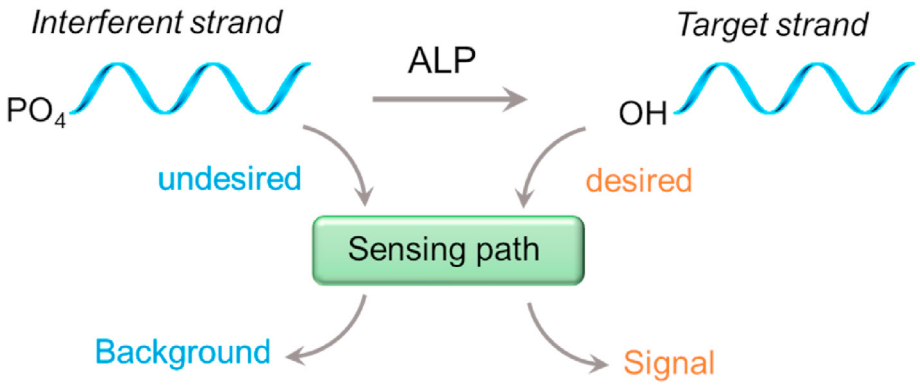

Scheme 1. A schematic depiction of the conventional design to detect the activity of ALP.

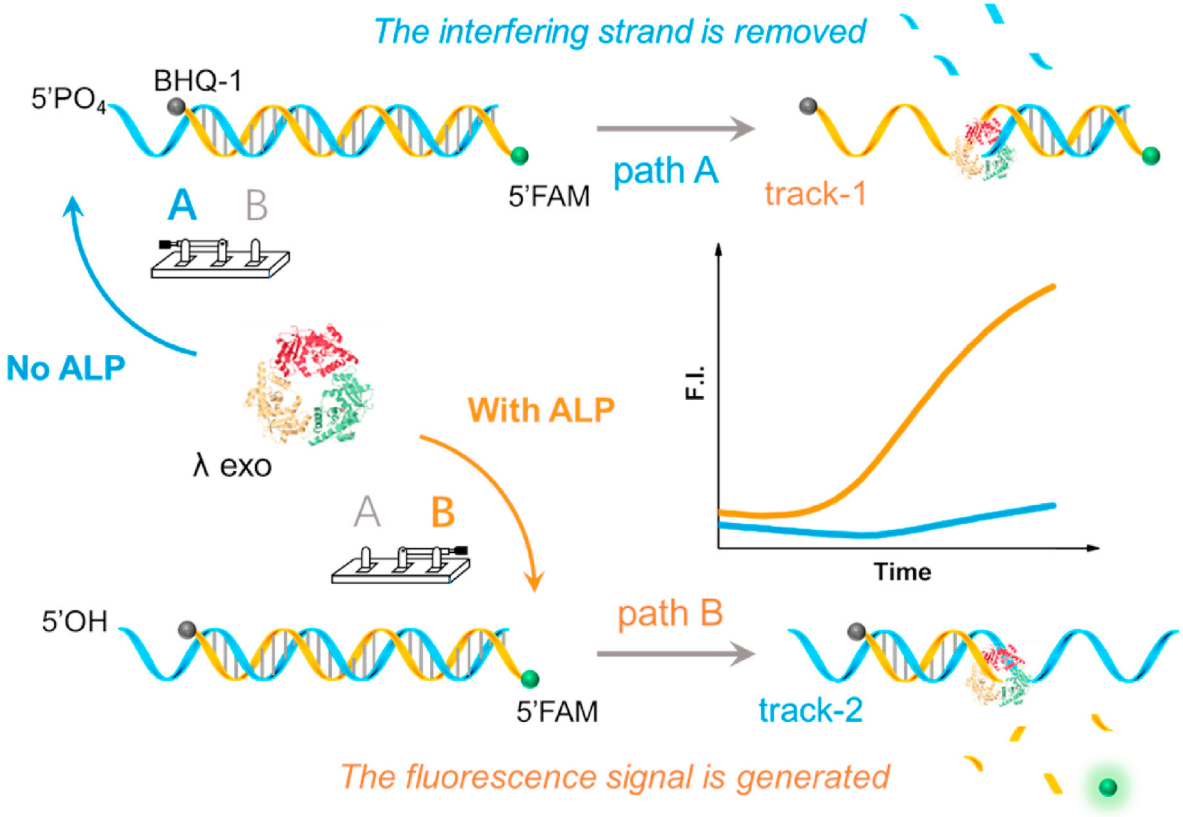

Fig. 1. A schematic depiction of the path-choice-based biosensor (PCB) to detect the activity of ALP as the switch. Without ALP, λ exo tends to go through path A in PCB (blue). The green ball represents FAM, and the black ball represents BHQ-1. The fluorescence signal is weak (blue line on the right). With ALP, 5′-PO_4 is converted to 5′-OH and λ exo is switched to path B (the sensing path, orange). The fluorescence signal is strong (orange line on the right). (For interpretation of the references to color in this figure legend, the reader is referred to the Web version of this article.)

32 μL of water after heating and annealing were incubated with 5×10^{-5} U of ALP (1 μL) at 37 °C for 90, 60, 30 and 0 min. Then, the reaction system was added to 400 μL ELISA plate, respectively. After that, 2 μL of λ exo (1 U) was added, and fluorescence detection was performed immediately as above.

2.4. Optimization of the concentration of DNA tracks (Fig. S4)

5 μL of the probe (1 pmol, 2.5 pmol, 5 pmol, 10 pmol), 5 μL of the C-strand-7nt (1 pmol, 2.5 pmol, 5 pmol, 10 pmol), 2.5 μL of 10 × CutSmart buffer and 2.5 μL of 10 × λ exo buffer and 32 μL of water after heating and annealing were added to 400 μL ELISA plate, respectively. 1 μL of ALP (5×10^{-5} U) and 2 μL of λ exo (1 U) were added at the same time, and then the fluorescence detection was performed with the detection conditions as above.

2.5. Digestion of the tracks in PCB with or without ALP (Fig. 2B and Fig. 2C)

5 μL of the probe (2.5 pmol), 5 μL of the C-strand or C-strand-OH (2.5 pmol) with different 5'-PO4 overhang lengths (0-nt, 1-nt, 2-nt, 3-nt, 4-nt, 5-nt, 6-nt, 7-nt, 8-nt and 10-nt), 2.5 μL of 10 × CutSmart buffer and 2.5 μL of 10 × λ exo buffer and 35 μL of water after heating and annealing were added to the 400 μL ELISA plate,

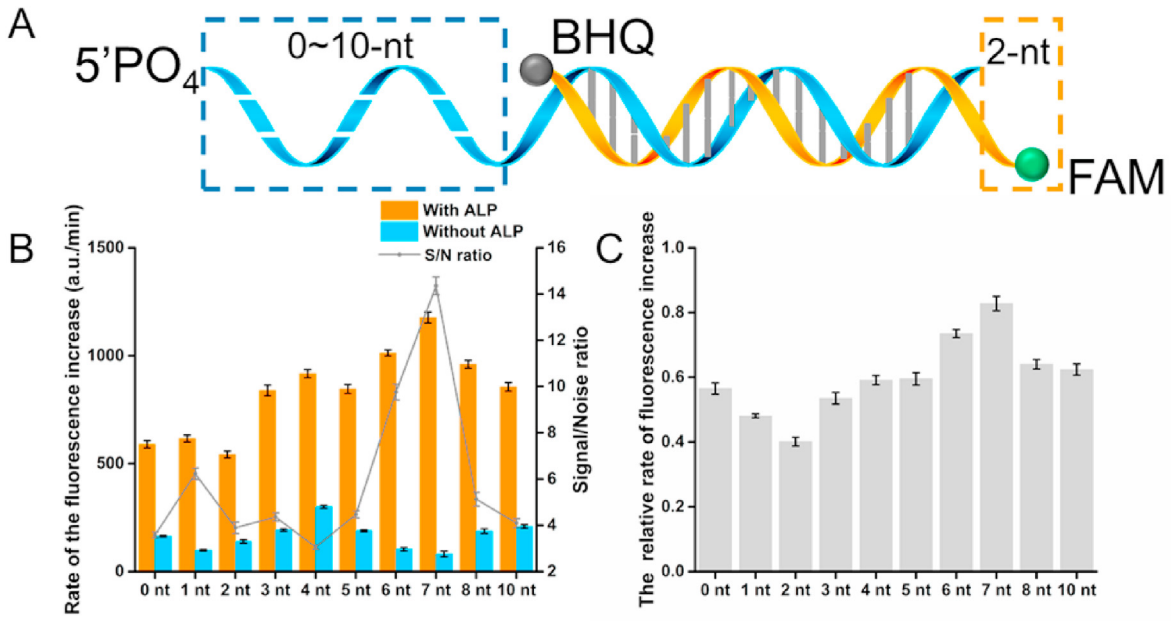

Fig. 2. **(A)** A schematic depiction of the tracks with different track-2 (C-strand) with 0–10 nt overhang at 5′-PO_4 end. **(B)** The rate of fluorescence increase of PCB with ALP (orange column, signal) and without ALP (blue column, noise) as the 5′-PO_4 overhang length changed. The signal/noise (S/N) ratio (grey line) was calculated for each length. **(C)** The relative rate of fluorescence increase of probe/C-strand with ALP to that of probe/C-strand-OH without ALP. The different lengths of the 5′ overhang in track-2 are marked on the horizontal axis. (For interpretation of the references to color in this figure legend, the reader is referred to the Web version of this article.)

Table 1
Sequences of the oligonucleotides used in this work.

Name	Sequence (5′>3′)
Track-1	
Probe[a]	FAM-**TC**TCCACAGACACATAC-BHQ
Track-2 with 5′-PO_4	
C-strand-0nt[b]	PO_4-GTATGTGTCTGTGGACCCGAGAGTAAG
C-strand-1nt	PO_4-CGTATGTGTCTGTGGACCCGAGAGTAAG
C-strand-2nt	PO_4-CCGTATGTGTCTGTGGACCCGAGAGTAAG
C-strand-3nt	PO_4-GCCGTATGTGTCTGTGGACCCGAGAGTAAG
C-strand-4nt	PO_4-CGCCGTATGTGTCTGTGGACCCGAGAGTAAG
C-strand-5nt	PO_4-TCGCCGTATGTGTCTGTGGACCCGAGAGTAAG
C-strand-6nt	PO_4-ATCGCCGTATGTGTCTGTGGACCCGAGAGTAAG
C-strand-7nt	PO_4-GATCGCCGTATGTGTCTGTGGACCCGAGAGTAAG
C-strand-8nt	PO_4-AGATCGCCGTATGTGTCTGTGGACCCGAGAGTAAG
C-strand-10nt	PO_4-CGAGATCGCCGTATGTGTCTGTGGACCCGAGAGTAAG
Track-2 with 5′-OH	
C-strand-0nt-OH	OH-GTATGTGTCTGTGGACCCGAGAGTAAG
C-strand-1nt-OH	OH-CGTATGTGTCTGTGGACCCGAGAGTAAG
C-strand-2nt-OH	OH-CCGTATGTGTCTGTGGACCCGAGAGTAAG
C-strand-3nt-OH	OH-GCCGTATGTGTCTGTGGACCCGAGAGTAAG
C-strand-4nt-OH	OH-CGCCGTATGTGTCTGTGGACCCGAGAGTAAG
C-strand-5nt-OH	OH-TCGCCGTATGTGTCTGTGGACCCGAGAGTAAG
C-strand-6nt-OH	OH-ATCGCCGTATGTGTCTGTGGACCCGAGAGTAAG
C-strand-7nt-OH	OH-GATCGCCGTATGTGTCTGTGGACCCGAGAGTAAG
C-strand-8nt-OH	OH-AGATCGCCGTATGTGTCTGTGGACCCGAGAGTAAG
C-strand-10nt-OH	OH-CGAGATCGCCGTATGTGTCTGTGGACCCGAGAGTAAG

[a] The TC in bold indicates that it forms the 2-nt overhang structure with track-2 strands.
[b] The bases underlined in the DNA sequences indicate that they are complementary to the probe.

respectively. For PCB with ALP, 2.5×10^{-4} U of ALP and 1 U of λ exo were added. For PCB without ALP, only 1 U of λ exo was added. Then put the plate into Synergy HTX for fluorescence measurement the same as above.

2.6. Verification of assumptions (Fig. 3B)

5 μL of the probe (2.5 pmol), 5 μL of the C-strand-7nt (2.5 pmol), 2.5 μL of 10 × CutSmart buffer and 2.5 μL of 10 × λ exo buffer and 35 μL of water after heating and annealing were added to 400 μL ELISA plate, respectively.1 U of λ exo was added and incubation at 37 °C for 30 min. Then, 5 μL of C-strand-7nt-OH (2.5 pmol) was added into the system, and fluorescence detection was performed immediately as above.

2.7. Agarose gel electrophoresis analysis (Fig. 3C)

Agarose gel electrophoresis was carried out using a 2.5% agarose gel at 110 V in a 1 × TBE buffer (90 mM Tris, 90 mM boric acid, 2 mM EDTA, pH 8.0). The samples were prepared in a 200 μl PCR tube with 30 μL of water, 2.5 μL of 10 × CutSmart reaction buffer, 2.5 μL of 10 × λ exo buffer, 7.5 μL of the probe (75 pmol) and 7.5 μl of the C-strand-7nt (75 pmol), which were incubated with 2 μL of λ exo (10 U) for 90 min, 60 min and 30 min (lane 1–3 in Fig. 3C) at 37 °C. The samples with either probe or C-strand-7nt and the sample without λ exo were control groups. Then, 6.67 μL of the sample solution and 1.33 μL of loading buffer were mixed and added to each well. After the separation in the electrophoresis apparatus (Junyi, Beijing, China), the gel was stained using the nucleic acid dye GelRed (Sangon Biotech Co., Shanghai, China). Then the gel was visualized at a wavelength of 590 nm using a Bio-Rad Universal Hood II gel imaging system (Bio-Rad, Shanghai, China).

2.8. Quantitative detection of ALP activity (Fig. 4A and Fig. 4D)

5 μL of the probe (2.5 pmol), 5 μL of the C-strand-7nt (2.5 pmol), 2.5 μL of 10 × CutSmart buffer and 2.5 μL of 10 × λ exo buffer and 35 μL of water after heating and annealing were added to 400 μL ELISA plate, respectively. 1 μL of ALP (final concentration 0 U L^{-1}, 0.05 U L^{-1}, 0.1 U L^{-1}, 0.2 U L^{-1}, 0.5 U L^{-1}, 1 U L^{-1}, 2 U L^{-1}, 5 U L^{-1}) and

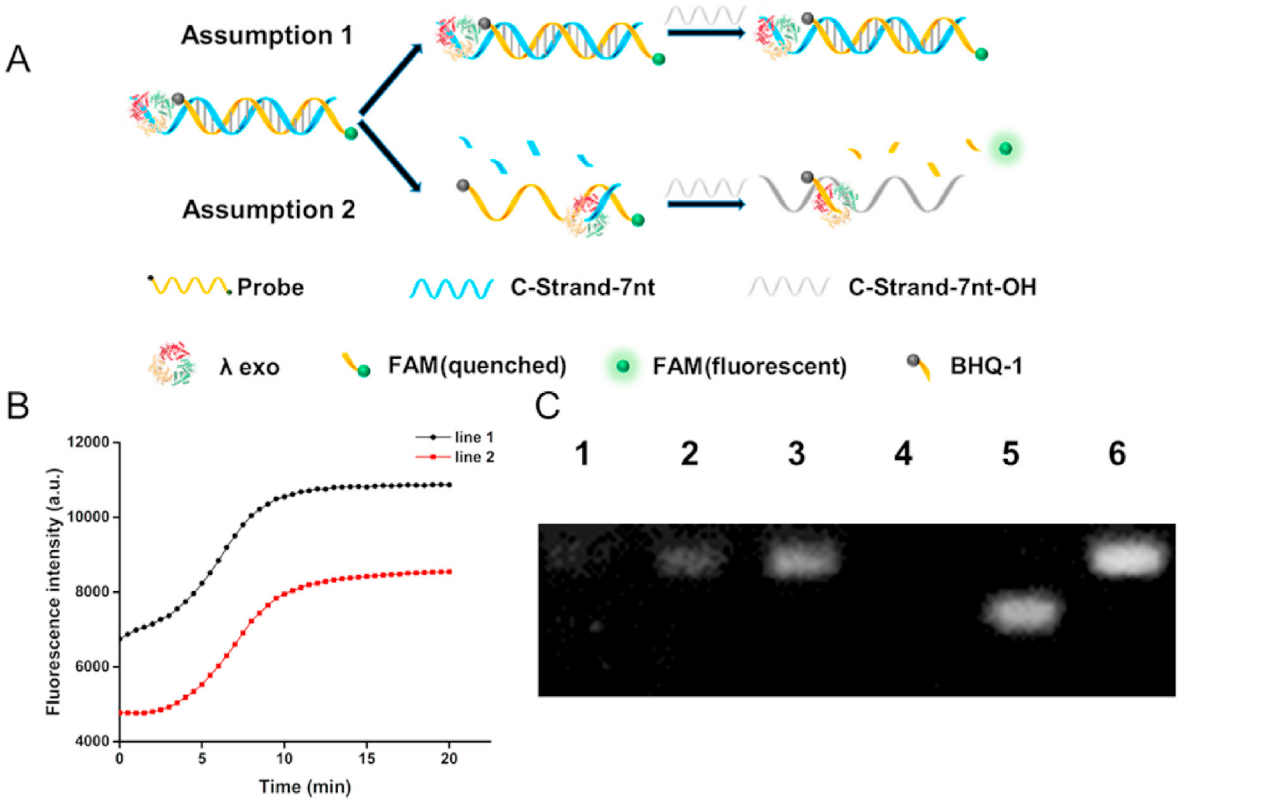

Fig. 3. **(A)** A schematic depiction of the reaction of probe/C-strand-7nt with λ exo and the subsequently added C-strand-7nt-OH. In assumption 1, λ exo is stacked by the 7-nt overhang in the C-strand in the first step and gives out weak fluorescence increase. In assumption 2, λ exo digests C-strand in the first step and digests the probe in the second step, resulting in a strong fluorescence increase. **(B)** Line 1 (control), the fluorescence response of the reaction of probe/C-strand–OH–7nt with λ exo. Line 2, the fluorescence response of the reaction in (A). **(C)** Probe/C-strand-7nt incubated with λ exo for 90 min (lane 1), 60 min (lane 2), 30 min (lane 3). Lane 4–6 are the controls without λ exo. Lane 4 is the probe (ssDNA). Lane 5 is C-strand-7nt (ssDNA) and lane 6 is probe/C-strand-7nt (dsDNA).

2 μL of λ exo (1 U) were added at the same time, and then the fluorescence detection was performed with the detection conditions as above.

2.9. Measurement of the stability of the method (Table S2)

5 μL of the probe (2.5 pmol), 5 μL of the C-strand-7nt (2.5 pmol), 2.5 μL of 10 × CutSmart buffer and 2.5 μL of 10 × λ exo buffer and 35 μL of water after heating and annealing were added to 400 μL ELISA plate, respectively. 1 μL of ALP (5×10^{-5} U) and 2 μL of λ exo (1 U) were added at the same time, and then the fluorescence detection was performed with the detection conditions as above. The detection in the condition above was performed for 6 times per day in different four days (total 24 times).

2.10. Measurement of the selectivity of the method (Fig. 4C)

5 μL of the probe (2.5 pmol), 5 μL of the C-strand-7nt (2.5 pmol), 2.5 μL of 10 × CutSmart buffer and 2.5 μL of 10 × λ exo buffer and 35 μL of water after heating and annealing were added to 400 μL ELISA plate, respectively. 1 μL of ALP, DNase I, T7 exo, Exo III, UDG (all the enzymes were 5×10^{-5} U), BSA (0.1 mg ml^{-1}) and a mixture of all proteins above (all the enzymes were 5×10^{-5} U and BSA was 0.1 mg ml^{-1}) were added, respectively. Then 2 μL of λ exo (1 U) was added. The fluorescence detection was performed with the detection conditions as above.

2.11. Inhibitor of ALP (Fig. 4C)

5 μL of the probe (2.5 pmol), 5 μL of the C-strand-7nt (2.5 pmol), 2.5 μL of 10 × CutSmart buffer and 2.5 μL of 10 × λ exo buffer and 35 μL of water after heating and annealing were added to 400 μL ELISA plate, respectively. 1 μL of ALP (5×10^{-5}U) and 1 μL of Na_3VO_4 (1.25 nmol) were mixed and incubated for 5 min and then added into the plate together with 2 μL of λ exo (1 U). The fluorescence detection was performed with the detection conditions as above.

2.12. Determination of ALP activity in biological samples (Fig. 4D)

Approximately 10^6 HELA cell samples were precipitated by centrifugation (3000 rpm, 5 min, 4 °C) and resuspended in 90 μL of cracking buffer (10 mM Tris-HCl, pH 7.0) on the ice. The mixture solution was then centrifuged at 12,000 rpm for 30 min at 4 °C to remove insoluble substances.

5 μL of the probe (2.5 pmol), 5 μL of the C-strand-7nt (2.5 pmol), 2.5 μL of 10 × CutSmart buffer and 2.5 μL of 10 × λ exo buffer and 35 μL of water after heating and annealing were added to 400 μL ELISA plate, respectively. Gradient cell lysate (with 200, 150, 100, 50, 10, and 0 cells) and 2 μL of λ exo (1 U) were added. And then the fluorescence detection was performed with the detection conditions as above.

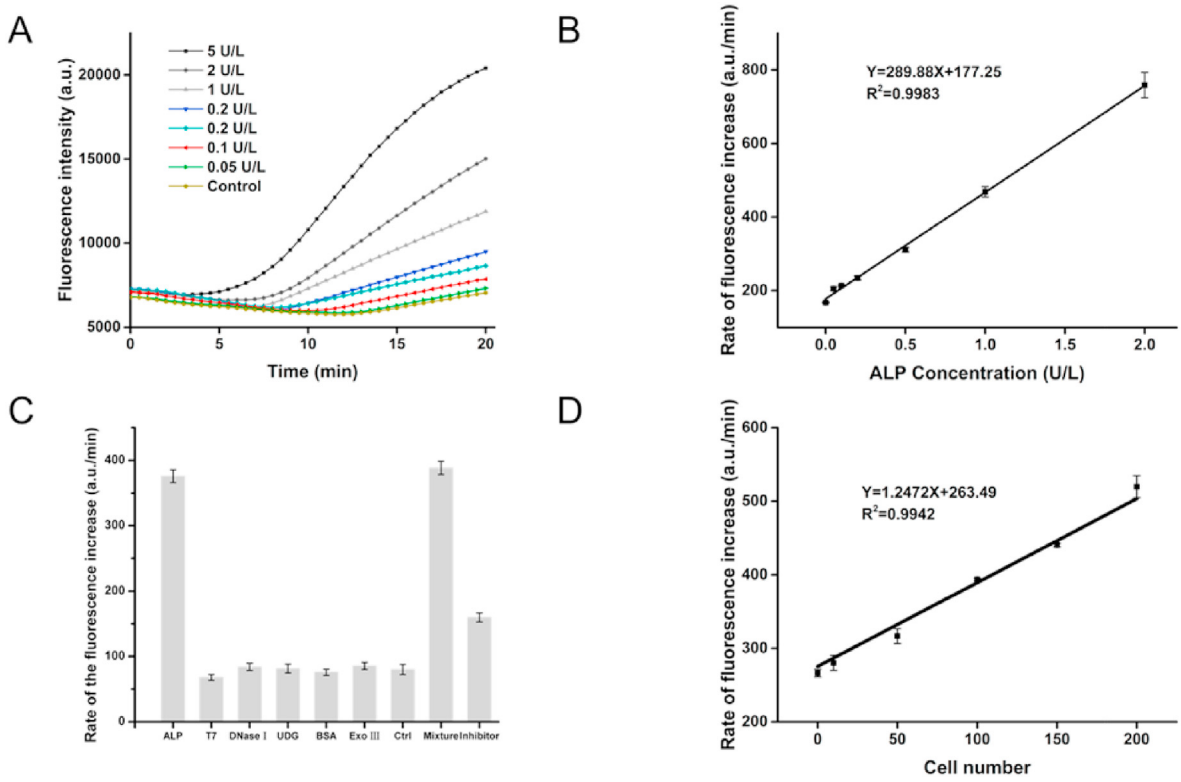

Fig. 4. **(A)** The fluorescence responses of PCB (probe/C-strand-7nt as the tracks) with different concentrations of ALP from 0 to 5 U L^{-1}. **(B)** The linear regression of the rate of fluorescence increase in (A) with ALP ranging from 0 to 2 U L^{-1} (0, 0.05, 0.1, 0.2, 0.5, 1, 2). The LOD can be calculated to be 0.014 U L^{-1} by 3σ K^{-1}. **(C)** The rate of fluorescence increase of PCB (probe/C-strand-7nt as the tracks) with different switches (1U L^{-1} of ALP, BSA, DNase I, T7 exo, Exo III, UDG and a mixture of above proteins). Ctrl means that there was no switch. Inhibitor means that ALP was added together with its inhibitor (25 μmol Na_3VO_4). **(D)** The linear regression of the rate of fluorescence increase with different cell number from 0 to 200 (0, 10, 50, 100, 150, 200). The LOD can be calculated to be 12 by 3σ K^{-1}.

3. Results and discussion

3.1. Design principle of the path-choice based biosensor

The design principle of the path-choice-based biosensor was shown in Fig. 1. The path-choice character was realized based on the novel property of λ exo as we recently reported [45,46]. λ exo was thought to only digest the substrate with 5'-PO_4. However, we found that λ exo could also digest the 5′-FAM ended strand with the two-nucleotide (2-nt) overhang structure (see detailed discussions in Fig. S1 and Table S1 in the Supporting Information) [45,46]. Moreover, λ exo has different activities to different 5′ ends, and the ranking of cleavage rates to different substrates is 5′-PO_4 > 5′-FAM > 5′-OH [45,46]. In PCB, we designed a dsDNA with two tracks. Track-1 is a single-stranded DNA (ssDNA) and acts as the fluorescent probe (orange strand in Fig. 1). In the probe, the fluorophore 5′-FAM (green ball in Fig. 1) is quenched by the quencher 3′-BHQ-1 (black ball in Fig. 1) through fluorescence resonance energy transfer, and the initial fluorescent signal is weak. Track-2 (named as C-strand, blue strand in Fig. 1) is a ssDNA with 5′-PO_4 and most of the sequence is complementary to the probe. There is a 2-nt overhang structure at the 5′-FAM end and 0-nt to 10-nt overhang structure at the 5′-PO_4 end (Fig. 2A).

In PCB, λ exo (symmetrical toroid homotrimer in Fig. 1) acts as the Pac-man to digest one of the tracks. The different choice of λ exo will result in its different behaviours on two paths. In PCB, ALP works as a switch that controls the path-choice of λ exo. As shown in Fig. 1, without ALP (No ALP), λ exo tends to bind with the 5′-PO_4 end and digest the C-strand due to the cleavage preference of λ exo we found. In this situation, λ exo walks on track-1 and digests track-2. We name this reaction as path A, which will remove the interferent strand and result in a weak fluorescent signal (blue line on the right in Fig. 1) as the track-1 (probe) is intact. While with ALP, the 5′-PO_4 in track-2 will be converted to 5′-OH. Then λ exo tends to choose to bind with the 5′-FAM end and digest the probe to depart FAM and BHQ-1, resulting in a strong fluorescent signal (orange line on the right in Fig. 1). In this situation, λ exo walks on track-2 and digests track-1. We name this reaction as path B. With the increasing activity of ALP in PCB, more λ exo will choose path B and give out more fluorescent signal. Thus, the rate of fluorescence increase is related to the activity of ALP. The great advantage of PCB over conventional ALP detection designs is that the interferent strand will be digested in path A and could hardly go into the sensing path (path B). In this way, the undesired background could be minimized compared with that in conventional designs. It's worth mentioning that the introduction of 5′-FAM is the key point to build PCB. Scheme S1 shows the design using 5′-PO_4 and 5′-OH tracks to build PCB. In the presence of ALP, both of the tracks are 5′-OH and λ exo could choose the two paths in the same probability so the signal will have a 50% discount.

3.2. Reaction condition and track structure optimization

We optimized the reaction condition to make the path-choice more selective. The preferred buffers for λ exo and ALP are λ exo buffer (67 mM Glycine-KOH, 2.5 mM $MgCl_2$, 50 μg/ml BSA, pH 9.4 @ 25 °C) and CutSmart (50 mM KAc, 20 mM Tris-Ac, 10 mM $Mg(Ac)_2$, 100 μg/ml BSA, pH 7.9 @ 25 °C), respectively. We tried to use them alone or mix them with 1:1. As shown in Fig. S2, the rate of fluorescence increase with ALP (as signal) or without ALP (as

background) was calculated respectively for the three buffers. The ratio of signal to background (S/N) estimated the selectivity of the method. The mixed buffer showed the best selectivity for the reaction and was chosen to be used in the following experiments.

Then, we systematically studied the structure of the 5′ end of the C-strand (track-2) on the activity of λ exo to further magnify the difference between the signal and background. The C-strands were designed to have the 5′ end with 0-nt to 10-nt overhang (Fig. 2A and Table 1). As shown in Fig. 2B, for the background (without ALP, blue column), the rate of fluorescence increase did not have much difference for different C-strands. And they were all much smaller than that of the signal (with ALP, orange column). This means that when there was no ALP in PCB, λ exo tended to distribute to the 5′-PO_4 end and choose path A as we proposed. When ALP was added in PCB (orange column), the rate of fluorescence increase became greater as the overhang prolonged from 0-nt to 7-nt. Longer overhang (from 7-nt to 10-nt) decreased the rate. As a result, the signal-to-background ratio of the fluorescence increase rate became the largest when the C-strand has 7-nt overhang (grey line). These results may be related to the influence of the overhang to λ exo and ALP together.

To exclude the influence of λ exo, we designed the C-strand-OH as another series of track-2 which has the same sequence as the corresponding C-strand but has 5′-OH end (Table 1). C-strand-OH could mimic the product of C-strand when all the 5′-PO_4 converted to 5′-OH by ALP. Then the relative rate of fluorescence increase of probe/C-strand with ALP to that of probe/C-strand-OH without ALP would reflect the influence of different overhang lengths on the activity of ALP. As shown in Fig. 2C, the relative rate fluorescence increase of 7-nt overhang is the closest to 1, which indicates that ALP has the most significant activity for this kind of track in the ten tracks tested.

After the tracks were chosen, we optimized the reaction time of ALP to the tracks before adding λ exo. By increasing the reaction time of ALP to the tracks, more 5′-PO_4 could be converted to 5′-OH. Then more λ exo could be switched to path B, resulting in a higher fluorescent signal. As shown in Fig. S3, the rate of fluorescence increase of PCB became faster as the reaction time of ALP to the tracks increased from 0 min to 90 min before adding λ exo. However, the rate was only increased by 0.13, 0.23 and 0.45 times at the expense of 30 min, 60 min and 90 min longer total reaction time of the method. To balance the reaction time and the sensitivity of the method, we chose to add ALP and λ exo to react with the tracks simultaneously when detecting the activity of ALP.

Also, the concentration of the tracks was optimized. As shown in Fig. S4, by increasing the concentration of the tracks (probe/C-strand), the rate of fluorescence increase of PCB became lager, while the S/N slightly decreased. As S/N of 20 nM and 50 nM of the tracks were similar and 50 nM had a better signal, we choose 50 nM of the tracks in PCB for ALP detection.

3.3. Confirmation of the path-choice behaviour of λ exo

Next, we tried to confirm that λ exo indeed chose path A or path B on different occasions. The choice of path B is apparent when the fluorescent signal increases fast. While the choice of path A is not as that apparent. λ exo was thought to have limited activity on the substrate with 5′-PO_4 overhang, which is similar to ssDNA [47]. However, in this experiment, λ exo could still distribute to (if not digest) the C-strand with a long 5′-PO_4 overhang. As shown in Fig. 3A, one assumption is that the 7-nt overhang in the C-strand stacked λ exo. Another assumption is that λ exo chose path A in which it walked on track-1 (probe) and digested track-2 (C-strand). We first incubated λ exo with the tracks (probe/C-strand-7nt) for 30 min, then added C-strand−OH−7nt ssDNA (sequence in Table 1). If λ exo was stacked (assumption 1), there will be a low fluorescent signal. If λ exo chose path A (assumption 2), as the C-strand-7nt was removed by λ exo, the probe could be free to hybridize with newly added C-strand-7nt-OH and form dsDNA. Then λ exo could digest the probe in the dsDNA (probe/C-strand-7nt-OH) and gives out a fluorescent signal. As shown in Fig. 3B, the rate of fluorescence increase of this experiment (line 2) is similar to the control that directly use λ exo to digest probe/C-strand−OH−7nt (line 1). This result indicated that assumption 2 occurred and λ exo indeed chose path A with the tracks probe/C-strand-7nt without ALP.

The choice of λ exo in verified assumption 2 is not a canonical property. To confirm it, we further tested the production with agarose gel electrophoresis. As shown in Fig. 3C, probe/C-strand-7nt was digested for 90 min (lane 1), 60 min (lane 2) and 30 min (lane 3). Lane 4 (probe), lane 5 (C-strand-7nt) and lane 6 (probe/C-strand-7nt) were the controls without λ exo digestion. As there is a quencher (BHQ-1) on the probe, the ssDNA probe band could hardly be seen on the gel. With increasing digestion time, the band of the probe/C-strand-7nt was dimmer (from lane 3 to lane 1). And the product band could not be seen, which indicates the product was the probe (as in lane 4). Thus, we confirmed that the C-strand-7nt with a 5′-PO_4 overhang was truly digested by λ exo. Digestion of the long protruded 5′-PO_4 overhang in dsDNA substrate is a novel finding for the property of λ exo. We guessed that in the 5′ end path-choice model (5′-PO_4 and 5′-FAM in this case) in dsDNA, λ exo might show preference on the 5′-PO_4 even it is on the ssDNA part. This property is expected to be further investigated in the future.

3.4. Application of the path-choice based biosensor to ALP detection in biological samples

Then we applied PCB to detect ALP in real practice. Firstly, we chose probe/C-strand-7nt as the track and tested a series of ALP with different concentrations from 0 to 5 U L^{-1} (0, 0.05, 0.1, 0.2, 0.5, 1, 2, 5) to calculate the LOD of this method. As shown in Fig. 4A, with the increasing concentrations of ALP, the rate of fluorescence increase became larger. The linear range is 0.05−2 U L^{-1} and the LOD is 0.014 U L^{-1} (3σ K^{-1}) based on the linear regression equation in Fig. 4B. We need only 20 min to complete the reaction, and the whole process of the method could be done within 30 min. The stability of the method was studied with the measurement of ALP with 2 U L^{-1} for 6 times per day in different four days (total 24 repeats). The results in Table S2 showed that the RSD (relative standard error) ranged from 2.5% to 2.8% for intraday measurements and 2.8% for interday measurements. The selectivity of PCB to different proteins was shown in Fig. 4C. Nucleases, which consists of endonuclease and exonuclease, may provide the greatest interference to the method based on DNA biosensors. Thus, the interferent proteins tested included a non-related protein (bovine serum albumin, BSA), an endonuclease (DNase I), a 5′ exonuclease (T7 exonuclease, T7 exo), a 3’ exonuclease (Exonuclease III, Exo III) and another enzyme (Uracil glycosylase, UDG). All the interferent proteins tested had a similar signal to the control. We also mixed these proteins with ALP and added them into PCB. As shown in the seventh column in Fig. 4C, the signal is similar to that with ALP alone. Thus, PCB showed high selectivity towards different proteins, and ALP detection was not affected by the interferent proteins. To our knowledge, the nucleases, which wildly exist in the real samples such as cell lysate and serum, are for the first time considered in the selectivity detection of ALP (see in Table S3). We also tested the inhibition effect of Na_3VO_4, which is commonly used to inhibit ALP activity. As shown in the rightmost column in Fig. 4C, Na_3VO_4 significantly decreased the rate of fluorescence increase, which demonstrated that PCB could be applied to ALP inhibitor screening.

The high selectivity ensured the application for real sample detection. We tested the activity of ALP extracted from HELA cells to

evaluate the practicability in the biological application. As shown in Fig. 4D, the activity of ALP showed excellent linearity with the cell number ranging from 0 to 200. Our method could detect the activity of ALP in as low as 12 cells (3σ K^{-1}), which is comparable with the method with complicated designs [28,29].

4. Conclusion

In summary, we proposed a novel path-choice-based biosensor (PCB) and used ALP as the switch to control the path-choice of λ exo. To our knowledge, this is the first path selector using DNA as the tracks and an enzyme as the switch. PCB would work as a path selector and has the potential to be used as a component in the complicated DNA logic circuit in the future. PCB has overcome the background generation problem in conventional ALP detection with only one path, and it has been successfully applied to detect the activity of ALP. The detection method has high sensitivity (0.014 U L^{-1}), high selectivity, simple design and fast process (30 min). Compared to the existing fluorescence-based methods shown in Table S3, our method has overcome the shortages of poor sensitivity, long reaction time, special components requirements, and uncleared selectivity (see detailed discussion in the Supporting Information). Requiring no special nor harsh reactions conditions, our method offers a balance of speed and low detection limit and shows a good selectivity towards nucleases which commonly present in biological samples. These advantages ensured the detection of ALP in complicated biological samples such as HELA cell lysates. Therefore, our method is promising to have broad application prospects in ALP-related biological research. Potentially, our method could be used to directly detect ALP in eutrophic water bodies to indicate DIP levels. Also, our method could be used to detect enzymes, proteins and small molecules using ALP to generate the signal. Besides, we optimized the structure of the tracks and found that ALP has the best activity on the tracks with 5′-PO_4 7-nt overhang structure. We also discovered the unexpected property of λ exo that it could digest the 5′-PO_4 overhang strand in dsDNA. These findings may promote the studies on the property of ALP and λ exo.

CRediT authorship contribution statement

Jiarui Zhang: Conceptualization, Methodology, Investigation, Writing - original draft. **Wenbo Zhao:** Conceptualization, Methodology, Investigation, Writing - review & editing. **Wei Zhang:** Investigation. **Yizhou Liu:** Writing - review & editing. **Yang Qin:** Investigation. **Wenkai Zhang:** Investigation. **Zhiyuan Zhou:** Investigation. **Yujie Zhou:** Investigation. **Hongbo Wang:** Resources. **Xianjin Xiao:** Funding acquisition, Writing - review & editing. **Tongbo Wu:** Supervision, Conceptualization, Funding acquisition, Writing - review & editing.

Declaration of competing interest

The authors declare that they have no known competing financial interests or personal relationships that could have appeared to influence the work reported in this paper.

Acknowledgements

This work was financially supported by the National Natural Science Foundation of China (No. 21904045, 21705053 and 81871732), the Fundamental Research Funds for the Central Universities (HUST: No. 2019kfyXJJS169), Training Program of Innovation and Entrepreneurship for Undergraduates of Hubei province (No. 2020104870134).

Appendix A. Supplementary data

Supplementary data to this article can be found online at https://doi.org/10.1016/j.aca.2020.08.040.

References

[1] J.E. Coleman, Structure and mechanism of alkaline phosphatase, Annu. Rev. Biophys. Biomol. Struct. 21 (1) (1992) 441.
[2] C. Chen, J. Zhao, Y. Lu, J. Sun, X. Yang, Fluorescence immunoassay based on the phosphate-triggered fluorescence turn-on detection of alkaline phosphatase, Anal. Chem. 90 (5) (2018) 3505–3511.
[3] L.Y. Jin, Y.M. Dong, X.M. Wu, G.X. Cao, G.L. Wang, Versatile and amplified biosensing through enzymatic cascade reaction by coupling alkaline phosphatase in situ generation of photoresponsive nanozyme, Anal. Chem. 87 (20) (2015) 10429–10436.
[4] H. Agis, S. Schrockmair, C. Skorianz, M.B. Fischer, G. Watzek, R. Gruber, Platelets increase while serum reduces the differentiation and activity of osteoclasts in vitro, J. Orthop. Res. 31 (10) (2013) 1561–1569.
[5] F.Y. Tian, J. Zhou, R.J. Fu, Y.L. Cui, Q.Y. Zhao, B.N. Jiao, Y. He, Multicolor colorimetric detection of ochratoxin A via structure-switching aptamer and enzyme-induced metallization of gold nanorods, Food Chem. 320 (2020) 8.
[6] M. Cadkova, V. Dvorakova, R. Metelka, Z. Bilkova, L. Korecka, Verification of antibody labelling efficiency as an important step in ELISA/QLISA development, Monatsh. Chem. 147 (1) (2016) 69–73.
[7] S.F. Liu, W.J. Wei, X.Y. Sun, L. Wang, Ultrasensitive electrochemical DNAzyme sensor for lead ion based on cleavage-induced template-independent polymerization and alkaline phosphatase amplification, Biosens. Bioelectron. 83 (2016) 33–38.
[8] X.L. Peng, G. Luo, Z. Wu, W. Wen, X.H. Zhang, S.F. Wang, Fluorescent-magnetic-catalytic nanospheres for dual-modality detection of H9N2 Avian Influenza virus, ACS Appl. Mater. Interfaces 11 (44) (2019) 41148–41156.
[9] M. Shu, Y. Xu, X. Liu, Y.P. Li, Q.H. He, Z. Tu, J.H. Fu, S.J. Gee, B.D. Hammock, Anti-idiotypic nanobody-alkaline phosphatase fusion proteins: development of a one-step competitive enzyme immunoassay for fumonisin B-1 detection in cereal, Anal. Chim. Acta 924 (2016) 53–59.
[10] R.Y. Li, Q. Liu, Y. Jin, B.X. Li, Fluorescent enzyme-linked immunoassay strategy based on enzyme-triggered in-situ synthesis of fluorescent copper nanoclusters, Sensor. Actuator. B Chem. 281 (2019) 28–33.
[11] H.X. Li, R. Jin, D.S. Kong, X. Zhao, F.M. Liu, X. Yan, Y.H. Lin, G.Y. Lu, Switchable fluorescence immunoassay using gold nanoclusters anchored cobalt oxyhydroxide composite for sensitive detection of imidacloprid, Sensor. Actuator. B Chem. 283 (2019) 207–214.
[12] X. You, C. Huang, Y. Luo, G. Shi, T. Zhou, J. Deng, A smartphone-based platform for point-of-use determination of alkaline phosphatase as an indicator of water eutrophication, Mikrochim. Acta 187 (6) (2020) 354.
[13] C. Labry, D. Delmas, A. Herbland, Phytoplankton and bacterial alkaline phosphatase activities in relation to phosphate and DOP availability within the Gironde plume waters (Bay of Biscay), J. Exp. Mar. Biol. Ecol. 318 (2) (2005) 213–225.
[14] S. Duhamel, S.T. Dyhrman, D.M. Karl, Alkaline phosphatase activity and regulation in the North Pacific subtropical gyre, Limnol. Oceanogr. 55 (3) (2010) 1414–1425.
[15] R.H. Christenson, Biochemical markers of bone metabolism: an overview, Clin. Biochem. 30 (8) (1997) 573.
[16] U. Sharma, D. Pal, R. Prasad, Alkaline phosphatase: an overview, Indian J. Clin. Biochem. : Indian J. Clin. Biochem. 29 (3) (2014) 269–278.
[17] J. Huping, C. Jian, L. Wenying, W. Fangyuan, Z. Huipeng, L. Yongxin, Y. Cong, Nucleic acid-regulated perylene probe-induced gold nanoparticle aggregation: a new strategy for colorimetric sensing of alkaline phosphatase activity and inhibitor screening, ACS Appl. Mater. Interfaces 6 (3) (2014) 1979–1985.
[18] R. Chuanmin, W. Wei, G. Baohua, Detection of alkaline phosphatase using surface-enhanced Raman spectroscopy, Anal. Chem. 78 (10) (2006) 3379–3384.
[19] S. Lakra, V.J. Jadhav, S.R. Garg, Development of a chromatographic method for the determination of alkaline phosphatase activity in pasteurized milk, Food Anal. Method 9 (7) (2016) 2002–2009.
[20] I. Kosuke, K. Yusuke, A. Toshiharu, K.Y. Inoue, T. Yasufumi, S. Hitoshi, M. Tomokazu, Novel electrochemical methodology for activity estimation of alkaline phosphatase based on solubility difference, Anal. Chem. 84 (18) (2012) 7593.
[21] S.J. Li, C.Y. Li, Y.F. Li, J.J. Fei, P. Wu, B. Yang, J. Ou-Yang, S.X. Nie, Facile and sensitive near-infrared fluorescence probe for the detection of endogenous alkaline phosphatase activity in vivo, Anal. Chem. 89 (12) (2017) 6854–6860.
[22] L. Dong, Q.Q. Miao, Z.J. Hai, Y. Yuan, G.L. Liang, Enzymatic hydrogelation-induced fluorescence turn-off for sensing alkaline phosphatase in vitro and in living cells, Anal. Chem. 87 (13) (2015) 6475–6478.
[23] H. Li, Q. Yao, F. Xu, Y. Li, D. Kim, J. Chung, G. Baek, X. Wu, P.F. Hillman, E.Y. Lee, H. Ge, J. Fan, J. Wang, S.-J. Nam, X. Peng, J. Yoon, An activatable AIEgen probe for high-fidelity monitoring of overexpressed tumor enzyme activity and its application to surgical tumor excision, Angew. Chem. 59 (25) (2020) 10186–10195.
[24] J. Liu, D. Tang, Z. Chen, X. Yan, Z. Zhong, L. Kang, J. Yao, Chemical redox

modulated fluorescence of nitrogen-doped graphene quantum dots for probing the activity of alkaline phosphatase, Biosens. Bioelectron. 94 (2017) 271–277.
[25] F. Wang, C. Zhang, Q. Xue, H. Li, Y. Xian, Label-free upconversion nanoparticles-based fluorescent probes for sequential sensing of Cu(2+), pyrophosphate and alkaline phosphatase activity, Biosens. Bioelectron. 95 (2017) 21–26.
[26] J. Sun, H. Mei, F. Gao, Ratiometric detection of copper ions and alkaline phosphatase activity based on semiconducting polymer dots assembled with rhodamine B hydrazide, Biosens. Bioelectron. 91 (2017) 70–75.
[27] X.X. Huangfu, Y. Shen, A.Z. Yang, L.X. Liu, W. Luo, W.B. Zhao, Synthesis of water soluble CuGaS2/ZnS quantum dots for ultrasensitive fluorescent detection of alkaline phosphatase based on inner filter effect, Colloids Surf. B Biointerfaces 191 (2020) 6.
[28] L.J. Wang, Z.Y. Wang, C.Y. Zhang, Primer dephosphorylation-initiated circular exponential amplification for ultrasensitive detection of alkaline phosphatase, Analyst 143 (19) (2018) 4606–4613.
[29] F. Ma, W.J. Liu, L. Liang, B. Tang, C.Y. Zhang, Sensitive detection of alkaline phosphatase by dephosphorylation-initiated transcription reaction-mediated dual signal amplification, Chem. Commun. 54 (19) (2018) 2413–2416.
[30] F. Ma, M. Liu, C.Y. Zhang, Ligase amplification reaction-catalyzed assembly of a single quantum dot-based nanosensor for sensitive detection of alkaline phosphatase, Chem. Commun. 55 (61) (2019) 8963–8966.
[31] P. Miao, L.M. Ning, X.X. Li, Y.Q. Shu, G.X. Li, An electrochemical alkaline phosphatase biosensor fabricated with two DNA probes coupled with lambda exonuclease, Biosens. Bioelectron. 27 (1) (2011) 178–182.
[32] X.G. Liu, X.J. Xing, B. Li, Y.M. Guo, Y.Z. Zhang, Y. Yang, L.F. Zhang, Fluorescent assay for alkaline phosphatase activity based on graphene oxide integrating with lambda exonuclease, Biosens. Bioelectron. 81 (2016) 460–464.
[33] Y. Zhang, Y. Wang, S.F.A. Rizvi, Y.D. Zhang, Y.T. Zhang, X.Y. Liu, H.X. Zhang, Detection of DNA 3 '-phosphatase activity based on exonuclease III-assisted cascade recycling amplification reaction, Talanta 204 (2019) 499–506.
[34] X. Liu, Z.H. Cheng, S.Q. Zhang, N. Wu, T. Yang, M.L. Chen, J.H. Wang, Amplification strategy of silver nanoclusters with a satellite-nanostructure for substrate-free assay of alkaline phosphatase by ICP-ms, Anal. Chem. 92 (5) (2020) 3769–3774.
[35] X.J. Liu, X.Y. Li, X. Gao, L. Ge, X.Z. Sun, F. Li, A universal paper-based electrochemical sensor for zero-background assay of diverse biomarkers, ACS Appl. Mater. Interfaces 11 (17) (2019) 15381–15388.
[36] J.J. Guo, M.X. Gao, Y.L. Song, L. Lin, K.F. Zhao, T. Pan, D. Liu, Z. Zhu, C.Y.J. Yang, An allosteric-probe for detection of alkaline phosphatase activity and its application in immunoassay, Front. Chem. 6 (2018) 9.
[37] H.S. Liu, C.B. Ma, J. Wang, K.M. Wang, K.F. Wu, A turn-on fluorescent method for determination of the activity of alkaline phosphatase based on dsDNA-templated copper nanoparticles and exonuclease based amplification, Microchim. Acta 184 (7) (2017) 2483–2488.
[38] J.Y. Du, L.Q. Xiong, C.B. Ma, H.S. Liu, J. Wang, K.M. Wang, Label-free DNA hairpin probe for real-time monitoring of alkaline phosphatase activity, Anal. Methods 8 (25) (2016) 5095–5100.
[39] J.W. Little, An exonuclease induced by bacteriophage lambda. II. Nature of the enzymatic reaction, J. Biol. Chem. 242 (4) (1967) 679–686.
[40] C.X. Song, X.H. Yang, K.M. Wang, Q. Wang, J.B. Liu, J. Huang, M.G. Zhou, X.C. Guo, Steric hindrance regulated supramolecular assembly between beta-cyclodextrin polymer and pyrene for alkaline phosphatase fluorescent sensing, Spectroc. Acta Pt. A-Molec. Biomolec. Spectr. 156 (2016) 131–137.
[41] Y. He, C. Wang, Q. Zhao, Y. Zhang, A. Chen, J. Pang, Q. Fang, Y. Cui, B. Jiao, Facile and sensitive fluorescence sensing of alkaline phosphatase activity using NMM/G-quadruplex, Talanta 172 (2017) 171–175.
[42] H. Wang, C. Ma, Z. Li, K. Wu, An exonuclease-assisted fluorescence sensor for assaying alkaline phosphatase based on SYBR Green I, Mol. Cell. Probes 45 (2019) 26–30.
[43] H.Y. Zhou, C.Y. Tong, B. Li, B. Liu, C.Y. Peng, J.L. Fan, W. Wang, An ultrasensitive and simple method for alkaline phosphatase assay and targeted natural compound screening in vitro, Anal. Bioanal. Chem. 410 (21) (2018) 5219–5228.
[44] C.B. Ma, H.S. Liu, K.F. Wu, M.J. Chen, H.L. He, K.M. Wang, K. Xia, A turn-on fluorescence assay of alkaline phosphatase activity using a DNA-silver nanocluster probe, New J. Chem. 42 (6) (2018) 4331–4336.
[45] T. Wu, Y. Yang, W. Chen, J. Wang, Z. Yang, S. Wang, X. Xiao, M. Li, M. Zhao, Noncanonical substrate preference of lambda exonuclease for 5′-nonphosphate-ended dsDNA and a mismatch-induced acceleration effect on the enzymatic reaction, Nucleic Acids Res. 46 (6) (2018) 3119–3129.
[46] T.B. Wu, W. Chen, Z.Y. Yang, H.C. Tan, J.Y. Wang, X.J. Xiao, M.Y. Li, M.P. Zhao, DNA terminal structure-mediated enzymatic reaction for ultra-sensitive discrimination of single nucleotide variations in circulating cell-free DNA, Nucleic Acids Res. 46 (4) (2018) 10.
[47] J.W.J.G.A. Little, Analysis, Lambda exonuclease. 2 (1981) 135–145.